Check for updates

Modulated synthesis of cesium phosphomolybdate encapsulated in hierarchical porous UiO-66 for catalysing alkene epoxidation†

Dianwen Hu, [ID] *[ab] Songsong Miao,[c] Pengfei Zhang,[d] Siyuan Wu,[e] Yu-Peng He [ID] [ab] and Qingwei Meng [ID] *[ab]

The hybrid composite of cesium phosphomolybdate (CsPM) encapsulated in hierarchical porous UiO-66 (HP-UiO-66) was synthesized using a modulated solvothermal method. A variety of characterization results demonstrated that the pore size distribution of CsPM@HP-UiO-66 is broader than traditional microporous CsPM@UiO-66 and cesium phosphomolybdate clusters are uniformly distributed in the octahedral cages of HP-UiO-66. The catalytic properties of the hybrid composite were investigated in alkene epoxidation reaction with *tert*-butyl hydroperoxide (*t*-BuOOH) as an oxidant. CsPM@HP-UiO-66 showed much higher catalytic activity for the alkene epoxidation reaction in comparison with the reference catalysts and could be easily reused by centrifugation and recycled for at least ten runs without significant loss in catalytic activity. The superior catalytic activity and stability of the hybrid composite CsPM@HP-UiO-66 should be mainly attributed to the hierarchical pores in the support HP-UiO-66 promoting the diffusion of alkene molecules, the uniform distribution of highly active CsPM clusters in the octahedral cages of HP-UiO-66, the introduction of cesium cations to form the insoluble cesium phosphomolybdate and the strong metal-support interactions (SMSI) between the CsPM clusters and the HP-UiO-66 framework.

Introduction

Metal–organic frameworks (MOFs) are a new class of crystalline porous materials that offer potential applications in gas storage and separation, sensing, biomedical application, and heterogeneous catalysis.[1–7] The use of MOFs as heterogeneous catalysts requires compositions and structures that can withstand reaction conditions without suffering irreversible structural damage so that they can be reused in successive runs. Several groups have reported that MOFs based on high valent metals (Al^{3+}, Ga^{3+}, In^{3+}, Fe^{3+}, Cr^{3+}, Sc^{3+}, Zr^{4+}, Ti^{4+}, …) exhibit good thermal and chemical stability in multiple catalytic reactions.[8] One of these favorite high valent metal-based MOFs used in

heterogeneous catalysis is UiO-66,[9–17] which is subjected to various post-synthetic modifications among others. Some of these possibilities will allow the introduction of additional functionalities, enabling these materials to be used as superior catalysts in different catalytic reactions.

Encapsulated polyoxometalates (POMs) clusters in the UiO-66 framework is a common modification strategy. Recently, Yang *et al.* synthesized phosphotungstic acid (HPT) encapsulated in UiO-66 hybrid composite. The obtained material showed high activity and reusability in the selective oxidation of cyclopentene to glutaraldehyde with hydrogen peroxide solution.[18] Bu group prepared the phosphomolybdic acid (HPM) encapsulated in UiO-66 hybrid composite, which showed a synergistic effect between active Mo species and UiO-66 supports, resulting in high oxidative desulfurization activity.[19,20] Jia group prepared a series of HPM@UiO-66 and TM-HPM@UiO-66 (TM = Fe, Co, Ni, Cu) composites. The obtained materials showed excellent catalytic activity and stability in various alkene epoxidation processes.[21,22]

Despite numerous advantages, the applications of conventional microporous MOFs are hindered by their micropore sizes in heterogeneous catalysis processes. The design of hierarchically porous MOFs (HP-MOFs) is crucial to achieving a controllable increase in MOF pore size up to mesopore or even macropore, which can improve reactant and product diffusion kinetics and increase the storage capacity of catalytically active

a Ningbo Institute of Dalian University of Technology, Ningbo 315016, China. E-mail: hudw_nbi@dlut.edu.cn; mengqw@dlut.edu.cn

b State Key Laboratory of Fine Chemicals, School of Chemical Engineering, Dalian University of Technology, Dalian 116024, China

c Changchun Institute of Applied Chemistry, Chinese Academy of Sciences, Changchun 130022, China

d State Key Laboratory of Catalysis, Dalian Institute of Chemical Physics, Dalian National Laboratory for Clean Energy, Chinese Academy of Sciences, Dalian 116023, China

e School of Chemistry and Molecular Engineering, East China University of Science and Technology, Shanghai 200237, China

sites.[23–27] Due to the structural stability of the framework, UiO-66 with mesopore or even macropore size has been successfully synthesized by different strategies. For instance, Zhou group proposed a relatively general method, ligand pyrolysis, which can controllably generate mesopores in UiO-66 derivatives.[28] Cai et al. used a monocarboxylic acid as the modulator to prepare hierarchically porous MOFs, including UiO-66 and its derivatives.[29] Yang and coworkers constructed regular macroporous channels and uniform macro porous walls in UiO-66 derivatives by systematically adjusting the feed ratio of different kinds of temples.[30] Moreover, the introduction of hierarchically porous structures in UiO-66 led to changes in the coordination state between $Zr_6O_4(OH)_4$ nodes and terephthalate (BDC) ligands, resulting in numerous defective sites that benefited the catalytic process.

Notably, researchers have concentrated their attention on combining POM clusters with hierarchically porous UiO-66 (HP-UiO-66) and using obtained materials in heterogeneous catalysis. Ye et al. reported that POM encapsulated in HP-UiO-66 composite showed much higher catalytic activity than POM encapsulated in traditional micropore UiO-66 in oxidative desulfurization reaction.[31] Zhang et al. synthesized Pt/UiO-66 with hierarchical pores. Such Pt/HP-MOF hybrid materials performed excellent catalytic activity and selectivity in catalytic hydrogenation reactions.[32] Cai et al. utilized defective HP-UiO-66 for the heterogenization of HPT. The resultant HPT-impregnated HP-UiO-66 (HPT/HP-UiO-66) led to prominent higher activity than the microporous counterpart in dye adsorption and the ring–opening reaction of styrene oxide with alcohol.[29] Feng et al. constructed HP-UiO-66 encapsulated ZrO_2 nanoparticles. The obtained ZrO_2@HP-UiO-66 produced excellent catalytic activity in the Meerwein–Ponndorf–Verley reaction.[28]

Inspired by the above-mentioned examples, herein, we tried to broaden the family of POM encapsulated in HP-UiO-66 composites for catalytic application in alkene epoxidation. HPM@HP-UiO-66 and CsPM@HP-UiO-66 composites were synthesized by the one-pot modulated solvothermal method. The obtained hybrid composites were characterized by a variety of means and the catalytic performance was investigated for alkene epoxidation reaction with t-BuOOH as oxidant. Under the test condition, hierarchically porous CsPM@HP-UiO-66 showed particularly high catalytic activity than traditional microporous CsPM@UiO-66. Besides, the leaching experiment indicates that the stability of CsPM@HP-UiO-66 is superior to HPM@HP-UiO-66. Moreover, CsPM@HP-UiO-66 could be easily recycled at least ten times without obvious loss in catalytic activity.

Experimental

Materials and instrumentation information

The complete list of chemicals, reagents, and instrumentation information are presented in the ESI.†

Catalyst preparation

Synthesis of HP-UiO-66. HP-UiO-66 was prepared according to the procedure reported in the literature with a slight modification.[19–22,29] Typically, 0.36 g $ZrCl_4$, 0.12 g BDC, and 9 g dodecanoic acid were dissolved in 60 mL DMF. After stirring for 2 h, the mixture was transferred to a Teflon-lined autoclave and kept at 393 K for 24 h. After cooling down to room temperature, the white precipitate was washed several times with DMF and acetone. Finally, the precipitate was dried overnight under a vacuum at 373 K.

Synthesis of HPM@HP-UiO-66 composite. HPM@HP-UiO-66 composite was prepared via the in situ synthesis method referring to a similar procedure as the pure HP-UiO-66. Typically, 0.36 g $ZrCl_4$, 0.12 g BDC, 0.06 g HPM, and 9 g dodecanoic acid were dissolved in 60 mL DMF. After stirring for 2 h, the mixture was transferred to a Teflon-lined autoclave and kept at 393 K for 24 h. After cooling down to room temperature, the precipitate was washed several times with DMF and acetone. Finally, the precipitate was dried overnight under a vacuum at 373 K. The loading amount of HPM in the hybrid composite was determined by the ICP-OES spectrometer as shown in Table S1.†

Synthesis of CsPM@HP-UiO-66 composite. CsPM@HP-UiO-66 composite was carried out by cation exchange. Firstly, twice synthetic equivalent HPM@HP-UiO-66 was added to 10 mL methanol solution of cesium acetate (12 mg mL^{-1}) at 333 K. After stirring for 3 h, the solids were separated by vacuum rotary evaporation method, then Soxhlet-extracted with methanol and dried overnight under vacuum at 373 K to obtain the CsPM@HP-UiO-66 composite, respectively. The loading amount of CsPM in the hybrid composite was determined by the ICP-OES spectrometer as shown in Table S1.†

Synthesis of microporous UiO-66, HPM@UiO-66 and CsPM@UiO-66 composites. For comparison, reference catalysts named UiO-66, HPM@UiO-66, and CsPM@UiO-66 composites were prepared according to the procedure reported in the literature with a slight modification.[19–22] Detailed synthesis routes are described in the ESI.†

Catalytic test. In a typical catalytic reaction procedure, 1.0 mmol of alkene, 3.0 mmol of t-BuOOH, 2.5 mL of solvent, and 10 mg of catalyst were added to a 25 mL round-bottom flask equipped with a stirring bar and a reflux condenser. The mixture was stirred for the required time at a specific temperature. The progress of the reaction was monitored by Shimadzu GC-2014C gas chromatograph equipped with a flame ionization detector (FID) using a SE-54 capillary column (30 m × 0.25 mm × 0.25 μm). After the reaction, the spent catalyst was isolated by centrifugation, washed with acetone repeatedly, and dried overnight at 373 K under vacuum.

Results and discussion

Catalyst characterization

The powder X-ray diffraction patterns of HP-UiO-66, HPM@HP-UiO-66, and CsPM@HP-UiO-66 composites are shown in Fig. 1. The XRD patterns of HP-UiO-66, HPM@HP-UiO-66, and CsPM@HP-UiO-66 composites are in good agreement with the simulated one, confirming the phase purity of these samples. Such a result may also provide initial evidence that the introduced phosphomolybdic acid or cesium cation might be uniformly scattered in hybrid composites.[19–22,28–32] The reference
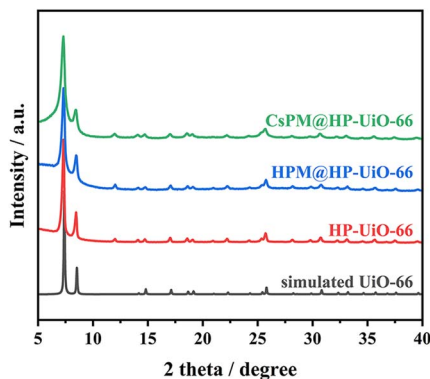
Fig. 1 XRD patterns of simulated UiO-66, HP-UiO-66, HPM@HP-UiO-66, and CsPM@HP-UiO-66 composites.

samples of microporous UiO-66, HPM@UiO-66 and CsPM@UiO-66 composites also show a similar XRD pattern as the simulated UiO-66 (Fig. S1†).

Nitrogen adsorption–desorption results of HP-UiO-66, HPM@HP-UiO-66, and CsPM@HP-UiO-66 composites are shown in Fig. 2A. All samples contain hysteresis loop, demonstrating the presence of mesopores.[23,33–35] As listed in Table 1, the calculated BET surface area of HP-UiO-66 is 868 $m^2 g^{-1}$, which is larger than HPM@HP-UiO-66 (706 $m^2 g^{-1}$) and CsPM@HP-UiO-66 (570 $m^2 g^{-1}$). Besides, the pore volume and pore size of HPM@HP-UiO-66 and CsPM@HP-UiO-66 also decreased. These results elucidate that the pore volume may be occupied by the POM clusters and cesium cationic. The pore size distributions calculated by the non-local density functional theory (NLDFT) method based on the adsorption branch from the BET isotherms show that the hybrid composites have similar pore size distribution to the parent HP-UiO-66, indicating that most of the
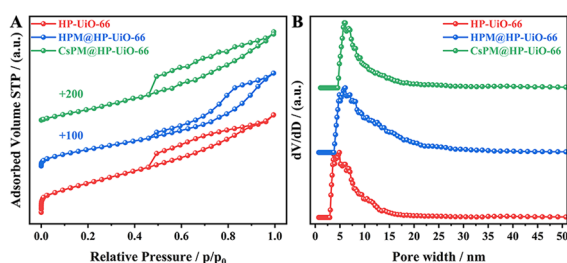
cages/channels in the HP-UiO-66 support are still open and accessible (Fig. 2B).[31,36–38] Meanwhile, the nitrogen adsorption–desorption result of the reference sample CsPM@UiO-66 is shown in Fig. S2,† the isotherm and the pore size distribution of the CsPM@UiO-66 present typical micropores feature.

The SEM images present in Fig. 3 show that the sample of HP-UiO-66, HPM@HP-UiO-66, and CsPM@HP-UiO-66 are distributed block structures, which were not uniform in size and irregular in morphology.[37,39] The individual crystals of reference sample UiO-66, HPM@UiO-66, and CsPM@HP-UiO-66 all have similar spherical morphologies, and appertaining to relatively uniform particles with an irregular shape, which is identified with the previous reports.[21,22]

The TEM images of CsPM@HP-UiO-66 are depicted in Fig. 4. No obvious CsPM crystalline can be found in the images, suggesting the high dispersion of CsPM clusters in the HP-UiO-66 framework. In addition, the images show typical worm-like mesopores, which is in good accordance with the nitrogen adsorption–desorption results mentioned above.[18,23,40]

Fig. 5A shows the FT-IR spectra of pure HP-UiO-66, HPM@HP-UiO-66, and CsPM@HP-UiO-66. In HP-UiO-66 and the hybrid composites, the absorption bands from 1300 to 1750 cm^{-1} are primarily assigned to the stretching vibration of the carbonyl and carboxylate in organic linkers. Besides, the absorption peaks around 757 and 665 cm^{-1} correspond to the Zr–O bond in HP-UiO-66 and the hybrid composites.[21,22,33,41] Notably, a slight characteristic peak around 800 cm^{-1} is attributed to Mo–O_c–Mo (bridging oxygen) in HPM or CsPM clusters in the hybrid composites.

The UV-vis absorption spectra of HP-UiO-66, HPM@HP-UiO-66, and CsPM@HP-UiO-66 composites are displayed in
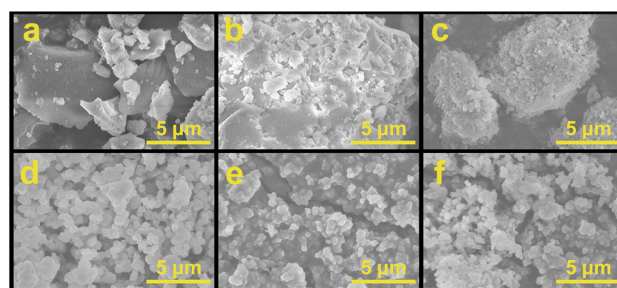

Fig. 2 N$_2$ adsorption–desorption (A) isotherms and (B) pore size distribution of HP-UiO-66, HPM@HP-UiO-66, and CsPM@HP-UiO-66 composites.

Fig. 3 SEM images of (a) HP-UiO-66, (b) HPM@HP-UiO-66 composite, (c) CsPM@HP-UiO-66 composite, (d) UiO-66, (e) HPM@UiO-66 composite and (f) CsPM@UiO-66 composite.

Table 1 The textural parameters derived from N$_2$ adsorption–desorption profiles

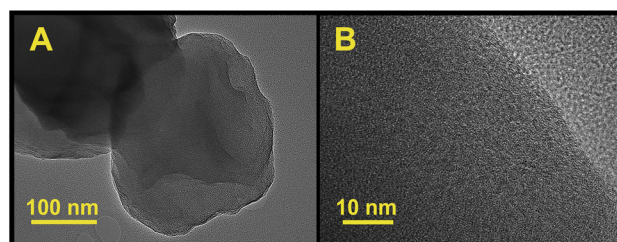| Sample	BET surface area ($m^2 g^{-1}$)	Pore volume ($cm^3 g^{-1}$)	Pore diameter (nm)
HP-UiO-66	868	0.62	6.1
HPM@HP-UiO-66	706	0.59	5.9
CsPM@HP-UiO-66	570	0.53	4.9

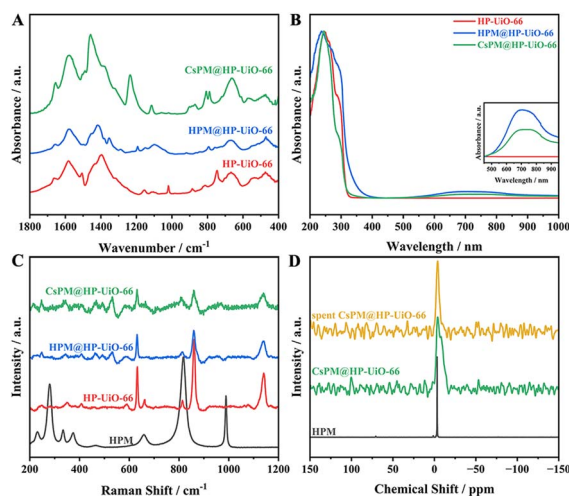**Fig. 4** TEM images of CsPM@HP-UiO-66 composite.

Fig. 5 (A) FT-IR and (B) UV-vis spectra of HP-UiO-66, HPM@HP-UiO-66 and CsPM@HP-UiO-66 composites; (C) Raman spectra of HPM, HP-UiO-66, HPM@HP-UiO-66 and CsPM@HP-UiO-66 composites; (D) ^{31}P MAS solid state NMR spectra of HPM, CsPM@HP-UiO-66 and spent CsPM@HP-UiO-66 composites.

Fig. 5B. Two absorption bands around 246 and 260 nm in the spectra of UiO-66 and hybrid composites are aroused by the ligand-to-metal charge transfer, suggesting the bonding between ligand and metal centers. Compared with HP-UiO-66, the spectra of the hybrid composites show an extra shoulder at around 300–400 nm in the spectra of hybrid composites, which is attributed to the Mo species in the hybrid composites. Moreover, the broad absorption in the range of 500–1000 nm may correspond to d–d transitions of Mo species (Fig. 5B inset), which also gave evidence of the presence of Mo species in HP-UiO-66.[19–22]

The Raman spectra of HPM, HP-UiO-66, HPM@HP-UiO-66 and CsPM@HP-UiO-66 composites are shown in Fig. 5C. The main characteristic peaks of the HPM structure observed at 990, 819, 658 and 280 cm^{-1} are assigned to ν_s(Mo–O$_d$), ν(Mo–O$_b$–Mo), ν_s(Mo–O$_c$–Mo) and ν_s(Mo–O$_a$) in HPM.[42–44] Besides, the prominent bands located at 1140, 863, and 634 cm^{-1} belong to the C–C symmetric ring breathing, OH bending with some contribution from C–C symmetric breathing and aromatic-ring in-plane bending in HP-UiO-66, respectively.[45] Notably, a weak signal associated with HPM appeared in the spectra of the hybrid composites, suggesting the existence of Mo species in them. Compared with the HP-UiO-66, a slightly blue shift is detected in the spectra of hybrid composites, indicating the existence of the interaction between HPM clusters and HP-UiO-66.[19,20,22]

The ^{31}P magic-angle spinning (MAS) solid state NMR spectra for HPM, CsPM@HP-UiO-66, and spent CsPM@HP-UiO-66 are shown in Fig. 5D. A narrow signal was observed at −3.3 ppm for HPM, assigned to the characteristic P atom in the Keggin structure of HPM.[22,44] In addition, a broad signal at −4.4 ppm is shown in the spectrum of CsPM@HP-UiO-66, which indicates the coordinated environment of the P atom in HPM remains well after the preparation of the hybrid composite. The upfield

shift and the peak broadening of the ^{31}P resonance signal reveal the existence of interaction between HPM clusters and the framework of HP-UiO-66.[22,41]

The X-ray photoelectron spectroscopy (XPS) results of HPM, HP-UiO-66, and the hybrid composites are presented in Fig. 6. Two significant peaks at 236.5 and 233.3 eV are shown in the Mo 3d spectrum of HPM (Fig. 6A), which is attributed to the Mo^{VI} 3d$_{3/2}$ and Mo^{VI} 3d$_{5/2}$.[19–22,41,46] As displayed in Fig. 6B, the characteristic peaks at 185.2 and 182.8 eV, are attributed to Zr 3d$_{3/2}$ and Zr 3d$_{5/2}$ in the HP-UiO-66 framework.[19,20,22] Notably, the binding energy of Mo 3d in CsPM@HP-UiO-66 shows an obvious negative shift to that of HPM, which provides strong evidence that multiple interactions should exist between the framework of HP-UiO-66 and the encapsulated CsPM units, leading to the partial electron transfer from HP-UiO-66 frameworks to CsPM units.

The above-mentioned characterization results strongly confirm that strong metal-support interactions (SMSI) should exist between the encapsulated CsPM clusters and the HP-UiO-66 framework.[19–22,41]

Alkene epoxidation

Firstly, the catalytic properties of POM@HP-UiO-66 composites were investigated for the epoxidation of cyclooctene with *t*-BuOOH as oxidant in tetrachloromethane as solvent (Table 2 and Fig. 7). The result proved that CsPM@HP-UiO-66 composite catalyze the epoxidation of cyclooctene under the test condition. Based on the calculated TOF value of different catalysts using
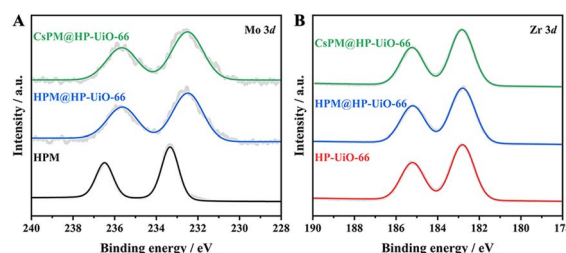

Fig. 6 XPS spectra for the binding energies of (A) Mo 3d in HPM, HPM@HP-UiO-66 and CsPM@HP-UiO-66 composites, (B) Zr 3d in HP-UiO-66, HPM@HP-UiO-66 and CsPM@HP-UiO-66 composites.

Table 2 Cyclooctene epoxidation performance of various catalysts[a]

Catalyst	Time (h)	Conversion (%)	TOF[b] (h^{-1})	Related work
Blank	12	21	—	This work
UiO-66	12	26	—	This work
CsPM@HP-UiO-66	6	36	14	This work
HPM@UiO-66-HCl	6	32	11	21
HPM@meso-OS[c]	6	58	4	51
HPM@COF-300c[c]	3	91	18	47

[a] Reaction condition: cyclooctene 1.0 mmol, *t*-BuOOH 3.0 mmol, tetrachloromethane 2.5 mL, catalyst 10 mg, reaction temperature 353 K. [b] TOF are expressed in mol(cyclooctene)·mol(Mo)$^{-1}$ h^{-1}. [c] Specific experimental conditions see related work.
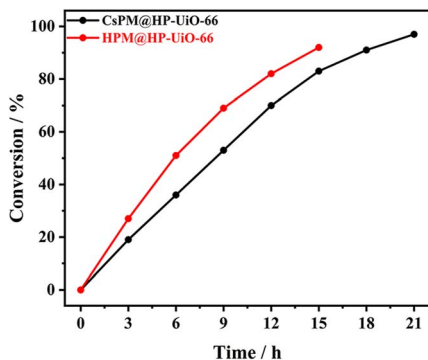
Fig. 7 Kinetic profile of cyclooctene epoxidation over HPM@UiO-66 and CsPM@HP-UiO-66 composites. Reaction condition: cyclooctene 1.0 mmol, t-BuOOH 3.0 mmol, tetrachloromethane 2.5 mL, catalyst 10 mg, reaction temperature 353 K.

various test conditions (Table 2), it is observed that the activity of CsPM@HP-UiO-66 (TOF 14 h^{-1}) is comparable to that of POM-based catalysts.[21,47] As displayed in Fig. 8A and B, hot filtration and recycling experiments proved that CsPM@HP-UiO-66 provided much higher stability against leaching. The spent CsPM@HP-UiO-66 was also characterized through XRD and ^{31}P MAS solid state NMR analysis (Fig. 5D and S3†). There are no significant differences between the fresh and spent catalysts, demonstrating that CsPM@HP-UiO-66 is a stable heterogeneous catalyst under the test condition.

As a reference catalyst, the catalytic properties of HPM@HP-UiO-66 were also tested under the same test condition. Notably, HPM@HP-UiO-66 showed a relatively high catalytic activity than CsPM@HP-UiO-66 (Fig. 7). However, the leaching test and recycling experiments indicated that HPM@HP-UiO-66 is not stable (Fig. 8C and D). Thus, it can be concluded that the introduction of cesium cation is an effective method for

stabilizing the POM clusters through the formation of an insoluble compound.[48–50]

To investigate the influence of the pore structure in alkene epoxidation, an additional experiment was carried out between CsPM@HP-UiO-66 and CsPM@UiO-66. As shown in Fig. S4,† CsPM@HP-UiO-66 exhibited preferable catalytic activity. From the result of nitrogen adsorption–desorption, both CsPM@HP-UiO-66, and CsPM@UiO-66 showed a large BET surface area, whereas the pore size distribution of CsPM@HP-UiO-66 is broader than CsPM@UiO-66. As mentioned in previous reports, increasing MOF pore size can improve reactant and product diffusion kinetics and increase the accessibility of catalytically active sites.[23–27] Thus, enlarging the pore size of the support UiO-66 is an efficient way to improve the catalytic properties of POM@UiO-66 composites.

The influence of solvent on the catalytic properties of CsPM@HP-UiO-66 was also evaluated. As shown in Table 3, the catalytic activity of CsPM@HP-UiO-66 is solvent-dependent.[21,51] Hereafter, tetrachloromethane is chosen as solvent to further study the catalytic property of CsPM@HP-UiO-66 for the epoxidation of other alkenes.

As shown in Table 4, CsPM@HP-UiO-66 can also catalyze the epoxidation of various alkenes. Linear alkenes like 1-octene and 1-decene could be converted to the corresponding epoxides but with relatively low conversion. Cyclic alkenes such as cyclooctene and cyclododecene could be oxidized in higher conversions with considerable selectivity of epoxides, suggesting that the oxygen transfer preferentially takes place at the electron-rich endocyclic position.[21] The specificity selectivity implies that only one catalytic route is principal during the catalytic process, as discussed later. Besides, CsPM@HP-UiO-66 is also active for the epoxidation of styrene (ST) with 31% conversion but 11% styrene oxide (SO) selectivity. Meanwhile, aldehydes are the main products with 44% selectivity of benzaldehyde (Bza) and 45% selectivity of phenylacetaldehyde (Pha). The lower selectivity of epoxides may attribute to the strong base property of cesium. Previous studies discovered that SO can easily convert to Pha with the existence of acid or base active sites (Scheme S1†).[52,53]

Based on previous reports, the epoxidation of alkenes over CsPM@HP-UiO-66 could also occur in different ways when t-BuOOH is used as oxidant. As described in Scheme S2,† it may
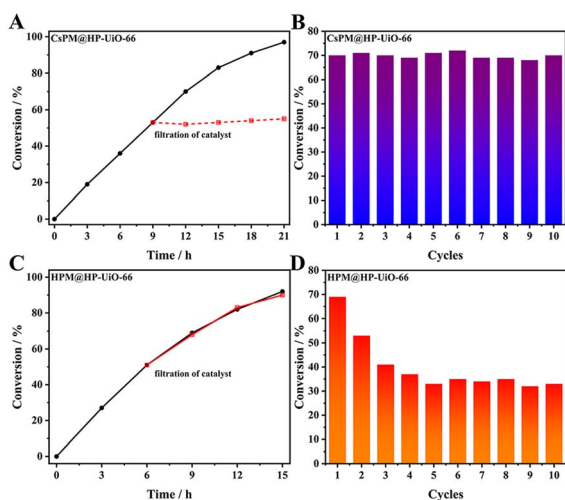

Fig. 8 Leaching experiments and recycling experiments of (A) and (B) CsPM@HP-UiO-66 and (C) and (D) HPM@HP-UiO-66 composites. Reaction conditions: cyclooctene 10 mmol, t-BuOOH 30 mmol, catalyst 100 mg, tetrachloromethane 25 mL, 353 K, 6 h (for recycling experiments).

Table 3 Cyclooctene epoxidation catalysed by CsPM@HP-UiO-66 in different solvent[a]

Solvent	Conversion (%)	TOF[b] (h^{-1})
Tetrachloromethane	70	12
1,2-Dichloroethane	34	6
Acetonitrile	28	5
Ethanol	10	2
1,4-Dioxane	5	1
Toluene	4	1

[a] Reaction condition: cyclooctene 1.0 mmol, t-BuOOH 3.0 mmol, solvent 2.5 mL, catalyst 10 mg, reaction temperature 353 K, 12 h. [b] TOF are expressed in mol(cyclooctene)·mol(Mo)$^{-1}$ h^{-1}.

Table 4 Alkene epoxidation catalysed by CsPM@HP-UiO-66[a]

Alkene	Conversion (%)	Selectivity (%)	TOF[b] (h^{-1})
Cyclooctene	70	96	12
Cyclododecene	32	95	6
1-Octene	6	99	1
1-Decene	4	99	1
Styrene	31	11	5

[a] Reaction condition: alkene 1.0 mmol, t-BuOOH 3.0 mmol, tetrachloromethane 2.5 mL, catalyst 10 mg, reaction temperature 353 K, 12 h. [b] TOF are expressed in mol(alkene)·mol(Mo)$^{-1}$ h^{-1}.

be directly activated by Mo species in POM to form Mo-OOR reactive intermediate, which is considered as an active intermediate for obtaining epoxide (route 1). Meanwhile, t-BuOOH may also be activated to form a radical species, which can usually result in the formation of other oxidation products (route 2).[21,54,55] Further controlling experiments demonstrated that the oxidation of cyclooctene over the CsPM@HP-UiO-66 catalyst could be slightly inhibited when hydroquinone was introduced into the reaction system as a radical scavenger. In this case, the conversion of cyclooctene slightly decreases from 97% to 92% (Fig. 9). Additionally, except for epoxide, other oxidation products could hardly be detected. These results also provide strong evidence that the radical-mediated route is present indeed but almost not the principal route under the test condition.

One-pot modulated synthesis is a widely used method to prepare HP-MOFs under solvothermal condition. Inspired by this, POM@HP-UiO-66 composites were also successfully synthesized in this work. By comparing the catalytic properties of the hierarchically porous CsPM@HP-UiO-66 and traditional micropores CsPM@HP-UiO-66, the hierarchically porous structure truly promotes the diffusion of reactant and product molecular under the test condition, which also enhances accessibility to POM sites. Based on the related literature,[18,21] the high stability of POM@UiO-66 could be mainly attributed to the size match between the POM clusters within the octahedral cages of UiO-66 frameworks. Typically, the size of HPM is about 10 Å, which fits the size of the octahedral cages (11 Å) of the UiO-66. Notably, the octahedral cages with smaller triangular windows (5–7 Å) can effectively prevent the loss of POMs.
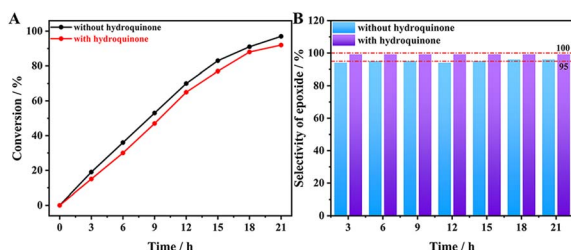
However, the introduction of mesopores changes the coordination state between the BDC ligands and $Zr_6O_4(OH)_4$ clusters. In that case, more defects can be found in the HP-UiO-66 framework, which increases the risk of POM leaching. The introduction of cesium cation to form insoluble cesium phosphomolybdate is effective to improve the stability of the POM@HP-UiO-66 catalyst to a certain extent. In addition, the SMSI between POM clusters and the UiO-66 frameworks, as proved by a variety of characterization results, should also play a positive role in fabricating highly stable hybrid composite catalysts.

Conclusion

In this work, the hybrid composite of CsPM@HP-UiO-66 was synthesized by one-pot modulated solvothermal method. A variety of characterization results demonstrated that the primary crystalline structure of UiO-66 support remains well after introducing mesopores, POMs, and cesium cation. CsPM@HP-UiO-66 shows excellent catalytic activity, selectivity, and stability for the epoxidation of a variety of alkenes with t-BuOOH as oxidant. The size-matched UiO-66 framework provides an ideal environment for stabilizing the introduced POM clusters by spatial confinement. Meanwhile, the additional introduction of cesium cation improves the anti-decomposition ability of active POM centers. Furthermore, the SMSI between the POM and UiO-66 framework is also beneficial to the stability of the CsPM@HP-UiO-66 catalyst. Further work is currently focused on studying the catalytic performance of these hybrid composites for application in other catalytic oxidation processes.

Author contributions

Dianwen Hu: investigation, methodology, formal analysis, writing – original draft, review & editing. Songsong Miao, Pengfei Zhang & Siyuan Wu: formal analysis. Yu-Peng He & Qingwei Meng: supervision.

Conflicts of interest

There are no conflicts to declare.

Acknowledgements

Fig. 9 (A) Conversion and (B) selectivity of cyclooctene epoxidation over CsPM@HP-UiO-66 composite. Reaction conditions: cyclooctene 1.0 mmol, t-BuOOH 3.0 mmol, catalyst 10 mg, tetrachloromethane 2.5 mL, 5 mg hydroquinone, 353 K.

Notes and references

1 J.-R. Li, R. J. Kuppler and H.-C. Zhou, *Chem. Soc. Rev.*, 2009, **38**, 1477–1504.
2 L. Yang, S. Qian, X. Wang, X. Cui, B. Chen and H. Xing, *Chem. Soc. Rev.*, 2020, **49**, 5359–5406.
3 A. H. Assen, O. Yassine, O. Shekhah, M. Eddaoudi and K. N. Salama, *ACS Sens.*, 2017, **2**, 1294–1301.

4 S. A. Noorian, N. Hemmatinejad and J. A. R. Navarro, *Microporous Mesoporous Mater.*, 2020, **302**, 110199.

5 A. Corma, H. García and F. X. Llabrés i Xamena, *Chem. Rev.*, 2010, **110**, 4606–4655.

6 J.-D. Yi, R. Xie, Z.-L. Xie, G.-L. Chai, T.-F. Liu, R.-P. Chen, Y.-B. Huang and R. Cao, *Angew. Chem., Int. Ed.*, 2020, **59**, 23641–23648.

7 Z. Guo, C. Xiao, R. V. Maligal-Ganesh, L. Zhou, T. W. Goh, X. Li, D. Tesfagaber, A. Thiel and W. Huang, *ACS Catal.*, 2014, **4**, 1340–1348.

8 T. Devic and C. Serre, *Chem. Soc. Rev.*, 2014, **43**, 6097–6115.

9 A. Dhakshinamoorthy, A. Santiago-Portillo, A. M. Asiri and H. Garcia, *ChemCatChem*, 2019, **11**, 899–923.

10 M. Zhang, H. Li, J. Zhang, H. Lv and G.-Y. Yang, *Chin. J. Catal.*, 2021, **42**, 855–871.

11 C. Freire, D. M. Fernandes, M. Nunes and V. K. Abdelkader, *ChemCatChem*, 2018, **10**, 1703–1730.

12 A. Haruna, Z. M. A. Merican and S. G. Musa, *J. Ind. Eng. Chem.*, 2022, **112**, 20–36.

13 K. Maru, S. Kalla and R. Jangir, *Dalton Trans.*, 2022, **51**, 11952–11986.

14 D.-Y. Du, J.-S. Qin, S.-L. Li, Z.-M. Su and Y.-Q. Lan, *Chem. Soc. Rev.*, 2014, **43**, 4615–4632.

15 P. Mialane, C. Mellot-Draznieks, P. Gairola, M. Duguet, Y. Benseghir, O. Oms and A. Dolbecq, *Chem. Soc. Rev.*, 2021, **50**, 6152–6220.

16 M. Samaniyan, M. Mirzaei, R. Khajavian, H. Eshtiagh-Hosseini and C. Streb, *ACS Catal.*, 2019, **9**, 10174–10191.

17 C. T. Buru and O. K. Farha, *ACS Appl. Mater. Interfaces*, 2020, **12**, 5345–5360.

18 X.-L. Yang, L.-M. Qiao and W.-L. Dai, *Microporous Mesoporous Mater.*, 2015, **211**, 73–81.

19 X.-M. Zhang, Z. Zhang, B. Zhang, X. Yang, X. Chang, Z. Zhou, D.-H. Wang, M.-H. Zhang and X.-H. Bu, *Appl. Catal., B*, 2019, **256**, 117804.

20 X. Chang, X.-F. Yang, Y. Qiao, S. Wang, M.-H. Zhang, J. Xu, D.-H. Wang and X.-H. Bu, *Small*, 2020, **16**, 1906432.

21 D. Hu, X. Song, S. Wu, X. Yang, H. Zhang, X. Chang and M. Jia, *Chin. J. Catal.*, 2021, **42**, 356–366.

22 D. Hu, X. Song, H. Zhang, X. Chang, C. Zhao and M. Jia, *Mol. Catal.*, 2021, **506**, 111552.

23 Z. Ai, L. Jiao, J. Wang and H.-L. Jiang, *CCS Chem.*, 2022, **4**, 3705–3714.

24 K.-Y. Wang, L. Feng, T.-H. Yan, S. Wu, E. A. Joseph and H.-C. Zhou, *Angew. Chem., Int. Ed.*, 2020, **59**, 11349–11354.

25 F. Meng, S. Zhang, L. Ma, W. Zhang, M. Li, T. Wu, H. Li, T. Zhang, X. Lu, F. Huo and J. Lu, *Adv. Mater.*, 2018, **30**, 11349–11354.

26 K. Li, S. Lin, Y. Li, Q. Zhuang and J. Gu, *Angew. Chem., Int. Ed.*, 2018, **57**, 3439–3443.

27 K. Shen, L. Zhang, X. Chen, L. Liu, D. Zhang, Y. Han, J. Chen, J. Long, R. Luque, Y. Li and B. Chen, *Science*, 2018, **359**, 206–210.

28 L. Feng, S. Yuan, L.-L. Zhang, K. Tan, J.-L. Li, A. Kirchon, L.-M. Liu, P. Zhang, Y. Han, Y. J. Chabal and H.-C. Zhou, *J. Am. Chem. Soc.*, 2018, **140**, 2363–2372.

29 G. Cai, P. Yan, L. Zhang, H.-C. Zhou and H.-L. Jiang, *Chem. Rev.*, 2021, **121**, 12278–12326.

30 J. Yang, K. Li and J. Gu, *ACS Mater. Lett.*, 2022, **4**, 385–391.

31 G. Ye, L. Hu, Y. Gu, C. Lancelot, A. Rives, C. Lamonier, N. Nuns, M. Marinova, W. Xu and Y. Sun, *J. Mater. Chem. A*, 2020, **8**, 19396–19404.

32 W. Zhang, Y. Liu, G. Lu, Y. Wang, S. Li, C. Cui, J. Wu, Z. Xu, D. Tian, W. Huang, J. S. DuCheneu, W. D. Wei, H. Chen, Y. Yang and F. Huo, *Adv. Mater.*, 2015, **27**, 2923–2929.

33 X.-S. Wang, L. Li, J. Liang, Y.-B. Huang and R. Cao, *ChemCatChem*, 2017, **9**, 971–979.

34 R. Xu, Q. Ji, P. Zhao, M. Jian, C. Xiang, C. Hu, G. Zhang, C. Tang, R. Liu, X. Zhang and J. Qu, *J. Mater. Chem. A*, 2020, **8**, 7870–7879.

35 A. H. Valekar, K.-H. Cho, S. K. Chitale, D.-Y. Hong, G.-Y. Cha, U. H. Lee, D. W. Hwang, C. Serre, J.-S. Chang and Y. K. Hwang, *Green Chem.*, 2016, **18**, 4542–4552.

36 P. Tian, X. He, W. Li, L. Zhao, W. Fang, H. Chen, F. Zhang, W. Zhang and W. Wang, *J. Mater. Sci.*, 2018, **53**, 12016–12029.

37 Z. Qi, Z. Huang, H. Wang, L. Li, C. Ye and T. Qiu, *Chem. Eng. Sci.*, 2020, **225**, 115818.

38 M.-Y. Zong, Z. Zhao, C.-Z. Fan, J. Xu and D. H. Wang, *Mol. Catal.*, 2023, **538**, 113007.

39 L. Zhou, F. Liu, J. Wang, R. Chen and Y. Chen, *CrystEngComm*, 2021, **23**, 2961–2967.

40 L.-B. Sun, J.-R. Li, J. Park and H.-C. Zhou, *J. Am. Chem. Soc.*, 2012, **134**, 126–129.

41 X. Song, D. Hu, X. Yang, H. Zhang, W. Zhang, J. Li, M. Jia and J. Yu, *ACS Sustainable Chem. Eng.*, 2019, **7**, 3624–3631.

42 S. Himeno, M. Hashimoto and T. Ueda, *Inorg. Chim. Acta*, 1999, **284**, 237–245.

43 A. J. Bridgeman, *Chem.–Eur. J.*, 2004, **10**, 2935–2941.

44 S. Silva, A. Chaumonnot, A. Bonduelle-Skrzypczak, F. Lefebvre, S. Loridant and V. Dufaud, *ChemCatChem*, 2014, **6**, 464–467.

45 C. Atzori, G. C. Shearer, L. Maschio, B. Civalleri, F. Bonino, C. Lamberti, S. Svelle, K. P. Lillerud and S. Bordiga, *J. Phys. Chem. C*, 2017, **121**, 9312–9324.

46 X. Song, Y. Yan, Y. Wang, D. Hu, L. Xiao, J. Yu, W. Zhang and M. Jia, *Dalton Trans.*, 2017, **46**, 16655–16662.

47 W. Gao, X. Sun, H. Niu, X. Song, K. Li, H. Gao, W. Zhang, J. Yu and M. Jia, *Microporous Mesoporous Mater.*, 2015, **213**, 59–67.

48 F. Jing, B. Katryniok, F. Dumeignil, E. Bordes-Richard and S. Paul, *J. Catal.*, 2014, **309**, 121–135.

49 J. C. S. Soares, A. H. A. Goncalves, F. M. Z. Zotin, L. R. Raddi de Araujo and A. B. Gaspar, *Mol. Catal.*, 2018, **458**, 223–229.

50 J. C. S. Soares, A. H. A. Goncalves, F. M. Z. Zotin, L. R. R. D. Araujo and A. B. Gaspar, *Catal. Today*, 2021, **381**, 143–153.

51 J. Wang, Y. Zou, Y. Sun, M. Hemgesberg, D. Schaffner, H. Gao, X. Song, W. Zhang, M. Jia and W. R. Thiel, *Chin. J. Catal.*, 2014, **35**, 532–539.

52 M.-L. Gou, J. Cai, W. Song, Y. Duan, Z. Liu and Q. Niu, *Microporous Mesoporous Mater.*, 2020, **297**, 110037.

53 X.-F. Zhang, J. Yao and X. Yang, *Microporous Mesoporous Mater.*, 2017, **247**, 16–22.

54 J. Hu, K. Li, W. Li, F. Ma and Y. Guo, *Appl. Catal., A*, 2009, **364**, 211–220.

55 J. Tang, Y. Zu, W. Huo, L. Wang, J. Wang, M. Jia, W. Zhang and W. R. Thiel, *J. Mol. Catal. A*, 2012, **355**, 201–209.